Edge localized modes (ELMs)

1996 Plasma Phys. Control. Fusion 38 105

(http://iopscience.iop.org/0741-3335/38/2/001)

Plasma Phys. Control. Fusion **38** (1996) 105–128. Printed in the UK

REVIEW ARTICLE

Edge localized modes (ELMs)

H Zohm

MPI für Plasmaphysik, EURATOM Association, D-85748 Garching, Germany

Received 14 August 1995, in final form 2 October 1995

Abstract. The phenomenology of edge localized modes (ELMs), an MHD instability occurring in the edge of H-mode plasmas in toroidal magnetic fusion experiments, is described. ELMs are important to obtain experimental control of the particle inventory of fusion plasmas. From an analysis of the ELM behaviour of different magnetic fusion experiments, three distinct types are identified, namely dithering cycles, type III and type I ELMs. A physical picture of these phenomena is established on the grounds of theoretical models put forward to describe the different ELM phenomena.

1. Introduction

In this article, the so-called edge localized modes (ELMs), an MHD instability occurring at the edge of H-mode plasmas, are discussed. The H-mode is a regime of enhanced confinement in toroidal magnetic fusion devices [1]. For a review of H-mode physics see, for example, the review articles [2, 3]. ELMs lead to a fast ($\approx$ ms) loss of energy and particles from the plasma edge. By this effect, the particle inventory of H-mode discharges with repetitive ELMs, so-called ELMy H-mode discharges, can be controlled experimentally. This provides a strong motivation for the study of ELMs. ELMs are observed in many different magnetic fusion experiments, so that a wide variety of ELM phenomena is reported. It is the aim of this article to review the experimental findings and theoretical models of ELMs and to establish a common classification together with a physical picture of the ELM phenomenon. The rest of the article is therefore organized as follows. In section 2, a phenomenological description of ELMs is given; based on the experimental results from various magnetic fusion experiments, a general classification is established. In section 3, we review existing theoretical models put forward to explain the physics of ELMs. Based on this discussion, a physical picture of ELMs is established in section 4. Section 5 gives a summary and conclusions.

2. Phenomenological description of ELMs

In this section, we review the experimental results from several fusion experiments and try to establish a common classification of the different ELM phenomena.

2.1. General phenomenology

Figure 1 shows time traces from ELMy H-mode discharges in ASDEX Upgrade. It can be seen that stored energy and density become stationary on the timescale of the confinement

0741-3335/96/020105+24$19.50

times of energy and particles, i.e. several 100 ms. This is generally not the case in ELM-free H-mode phases, in which the plasma density and also the impurity content rise steadily. In these cases, the increased radiated power from the core diminishes $P_{\rm sep}$, the energy flux through the separatrix:

$$P_{\rm sep} = P_{\rm tot} - \frac{{\rm d}W}{{\rm d}t} - P_{\rm rad}({\rm core}). \tag{1}$$

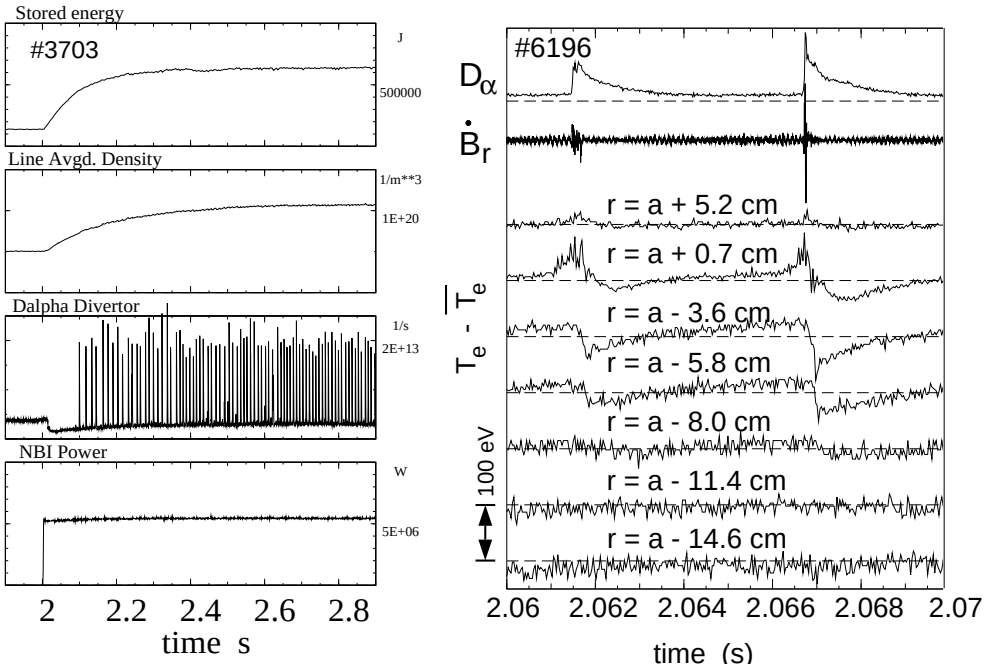

Figure 1. Stationary ELMy H-mode discharge in ASDEX Upgrade. The effect of ELMs on $T_{\rm e}$ in the plasma edge is shown for a similar discharge. Here, there is no effect of the ELMs on $T_{\rm e}$ for $r \leqslant 0.8a$.

It can be shown that the power threshold for the L–H and the H–L transitions are both governed by $P_{\rm sep}$ rather than by the total heating power $P_{\rm tot}$ [4], so that finally, $P_{\rm sep} \leqslant P_{\rm thr}^{\rm HL}$ holds and the plasma transits back to L-mode. In general, it is found that only ELMy H-modes become stationary (see e.g. [5]). This provides a strong motivation for analysing the ELM phenomenon.

In the right part of figure 1, the temporal evolution of the edge electron temperature is also shown for a similar discharge on an expanded timescale. The location of the separatrix is at $r = a$. Outside the separatrix, $T_{\rm e}$ increases during the ELM, indicating that the rapid outward transport induced by the ELM leads to a temporary heating of the SOL plasma. In the SOL, the optical depth is not sufficient to ensure an optically thick emission of the ECE radiation without the assumption of multiple reflections for the outermost channel. However, at $r = a + 2$ cm, the optical depth is already 2.5 and it is above 5 for all points inside the separatrix, ensuring optically thick emission. Inside the separatrix, the effect of the ELMs is to rapidly reduce $T_{\rm e}$. It can be seen that the effect of ELMs is really 'edge localized', i.e. $T_{\rm e}$ is not affected inside a certain radius $r_{\rm ELM}$ (in the case shown above, $r_{\rm ELM}/a \approx 0.8$). The ELM itself happens on a timescale of $\leqslant 1$ ms, which is faster than the

inverse of typical ELM repetition frequencies of $\nu_{\mathrm{ELM}} = 10$–200 Hz. Thus, ELMs appear as short, separated bursts. In addition, figure 1 shows the fluctuating magnetic field, measured by a pick-up coil in the outside midplane of the torus (signal $\dot{B}_r$). During ELMs, there is a high level of magnetic fluctuations, indicating that the rapid enhancement of transport is due to an MHD instability.

2.2. Classification of different ELM phenomena

The physical mechanisms for the different ELM phenomena are complex and no first-principles theory describing ELMs exists. We therefore give a phenomenological description based on the experimental observations of several magnetic fusion experiments operating in the H-mode and show that a common classification can be given.

2.2.1. DIII-D. The first classification of the different ELM phenomena was given for the DIII-D tokamak [6]. Three distinct types of ELM were found and numbered (the numbering indicating the historical sequence in which the ELM types were found). The original classification is based on three criteria: the dependence of the ELM repetition frequency ν_{ELM} on the heating power P; the occurrence of magnetic precursors; and the MHD stability with respect to the ideal ballooning criterion.

- *Type I ELMs.* the ELM repetition frequency ν_{ELM} increases with heating power. There is no detectable magnetic precursor oscillation. However, the level of broadband magnetic and density turbulent fluctuations increases prior to a type I ELM. Ideal ballooning analysis shows that the plasma edge is always close to the stability limit $\alpha \approx \alpha_{\mathrm{crit}}$ [7]. Type I ELMs appear as isolated sharp bursts on the D_α-signal.
- *Type II ELMs.* If, in a DIII-D discharge exhibiting type I ELMs, the shape of the plasma cross section is changed towards higher elongation and triangularity, the appearance of the ELMs may change: they become more frequent and the magnitude of the D_α-burst decreases. In this case, the plasma edge is found to be in the connection regime between the first and the second stable region of the ballooning diagram [8]. For type II ELMs, no information on the power dependence of ν_{ELM} or the MHD precursor activity exists.
- *Type III ELMs.* The ELM repetition frequency decreases with heating power. A coherent magnetic precursor oscillation of frequency $\nu_{\mathrm{prec}} \approx 50$–$70$ kHz is observed on magnetic probes located close to the plasma in the outboard midplane. A toroidal mode number of $n \approx 5$–10 was inferred. The plasma edge pressure gradient is significantly below the ideal ballooning limit, i.e. $0.3 \leqslant \alpha/\alpha_{\mathrm{crit}} \leqslant 0.5$ [9].

Thus, in a discharge where the heating power increased in steps, type III ELMs occur at heating power close to $P_{\mathrm{thr}}^{\mathrm{LH}}$, their frequency decreasing as P is increased until an ELM-free phase appears. At even higher P, type I ELMs occur, their frequency now increasing with P. Figure 2 shows an example.

In recent DIII-D experiments, it is clearly found that increasing the triangularity of the plasma has a strong tendency to stabilize type I ELMs. This method is used to produce long ELM-free phases and is one of the key elements that led to the discovery of the VH-mode [10]. Ideal ballooning analysis of these configurations indicates that the edge region has access to the second stability regime [11], thus again pointing to a link between the ideal ballooning stability and the occurrence of type I ELMs.

Another way sometimes used to characterize ELMs is by their D_α-signature. On DIII-D, single, isolated ELMs were called ‘giant ELMs’, whereas the type II ELMs were dubbed ‘grassy ELMs’. In contrast, on ASDEX and JET, highly frequent ELMs occurring at the

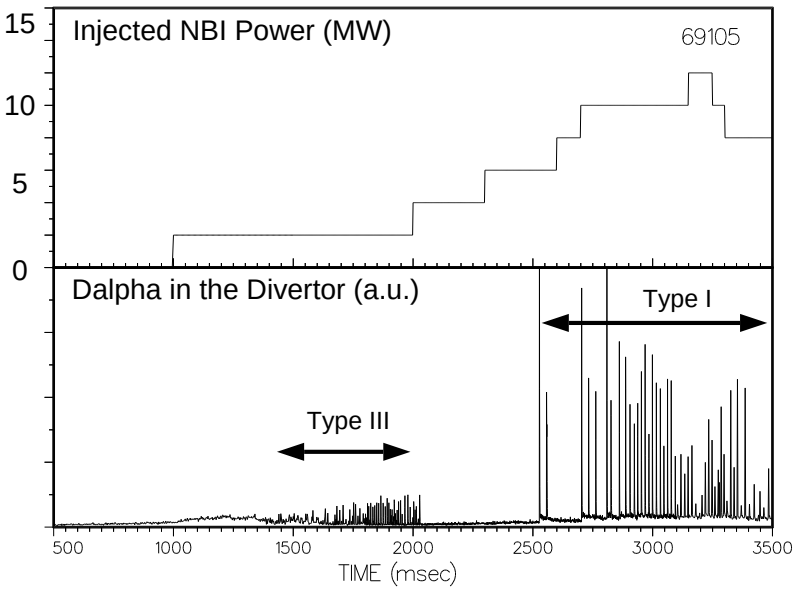

Figure 2. Typical sequence of ELMs during a power rise in DIII-D: at $P \approx P_{\rm thr}^{\rm LH}$, type III ELMs are found, at higher P, type I ELMs occur.

L–H transition were called grassy ELMs. In addition, the characterization by the D_α-signal is not unambiguous, because it depends on the divertor conditions. A somewhat extreme example for this is that in H-mode discharges with a detached divertor, where the energy and particle pulses are buffered in the divertor and do not reach the divertor plates, there is no significant change in the recycling during an ELM and consequently, no peak in the D_α-emission [12]. In this case, the characterization of ELMs by the D_α-signal fails completely.

In the following, we will therefore not use the D_α-signal for a classification. Instead, we shall apply the DIII-D classification to observations from other experiments and point out similarities and differences. After this, a more general classification, taking into account all the experimental results, will be given.

2.2.2. ASDEX. A detailed comparison of the ELM behaviour in ASDEX and DIII-D has been performed [9]. ELMs on ASDEX always exhibit a coherent magnetic precursor oscillation of frequency $\nu_{\rm prec} \approx 180$ kHz and poloidal mode number $m \approx 10$–15 [13]. In contrast, the ELM itself is a highly turbulent phenomenon with no clear coherent structure, but a high amplitude of the fluctuating magnetic field. This is shown in figure 3. The amplitude of the precursor is found to grow explosively before the ELM (see figure 3(*d*), which is an enlargement of the second hatched region of figure 3(*b*)). In other cases, the magnetic mode grows less strongly and then vanishes again without the subsequent occurrence of an ELM (see figure 3(*c*), enlargement of the first hatched region in figure 3(*b*)). It was concluded [13], that a critical amplitude of the perturbation must be reached to initiate an ELM. In addition to the occurrence of the magnetic precursor, the ELM repetition frequency on ASDEX decreases with heating power. These observations also hold for type III ELMs in DIII-D. It is therefore concluded that the ELMs appearing on ASDEX are of type III.

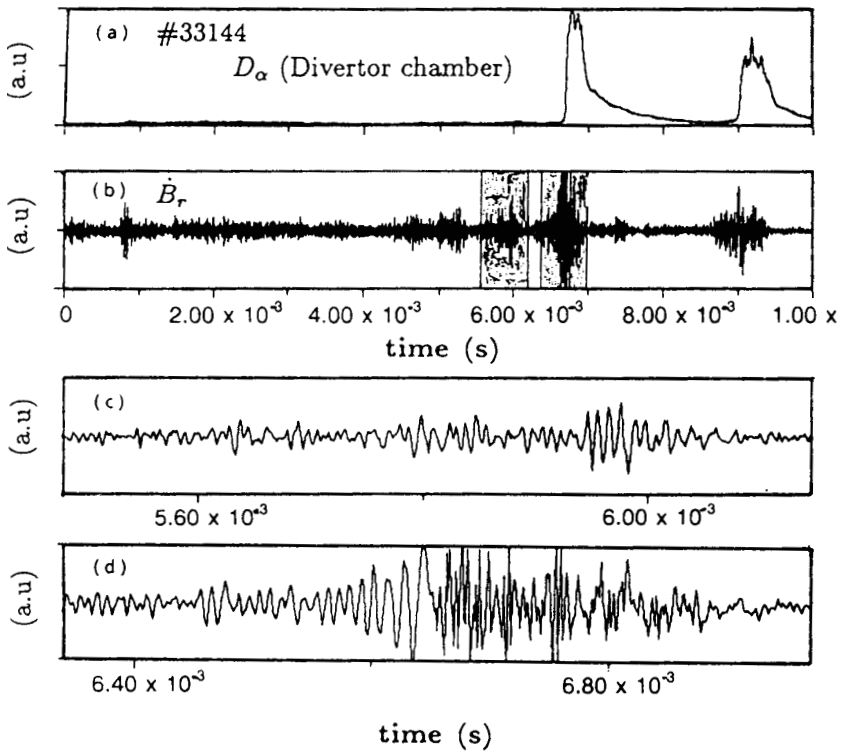

Figure 3. Type III ELMs on ASDEX: Mirnov coil measurements (*b*) show a coherent precursor. If it grows to sufficient amplitude (*d*), an ELM is initiated. The ELM itself is a highly turbulent phenomenon (*d*).

A pronounced difference exists with respect to the ballooning stability analysis. In ASDEX, only one type of ELM exists during a rise of heating power from the L–H threshold up to the highest available power. For the highest heating power, the plasma was analysed to reach the Troyon β-limit. In these discharges, the pressure gradient was close to the ideal ballooning limit everywhere with $\alpha/\alpha_{\rm crit} \approx 0.9$ in the edge region [14]. This is a clear contradiction to DIII-D, where type III ELMs are only observed at $\alpha/\alpha_{\rm crit} \leqslant 0.5$ and, at the ideal ballooning limit, type I ELMs occur.

Major differences between DIII-D and ASDEX are the different geometry and the size of the plasma cross section. Both tokamaks have a major radius of $R_0 = 1.65$ m, but ASDEX has a circular cross section of minor radius $a = 0.4$ m whereas DIII-D plasmas are normally elongated to $\kappa = 1.8$–2 and have a minor radius of $a = 0.63$ m. Experiments were carried out in DIII-D, during which plasmas with cross section close to the ASDEX shape and size were reproduced. In these discharges, only one type of ELM was found for heating powers from $P_{\rm thr}^{\rm LH}$ up to the β-limit, where the edge was close to the ideal ballooning limit, and it was identified as a type III ELM by its magnetic precursor oscillation, thus confirming the different ELM behaviour of ASDEX and DIII-D [9].

There are two possible effects of the different geometry and size of the poloidal cross section on the ELM physics. As the volume of the DIII-D plasma is higher than that of ASDEX by a factor of ≈ 3, a higher heating power can be applied, leading to higher

absolute values of the energy flux through the plasma edge at the same $\alpha/\alpha_{\rm crit}$ and therefore to potentially higher edge temperatures $T_{\rm e}(a)$. A second factor is that MHD stability analysis shows that elongation and triangularity strongly improve the ballooning stability. From the comparison of ASDEX and DIII-D, it is, however, not possible to find out which effect dominates the difference in the ELM physics.

From these differences, we can conclude that the ratio $\alpha/\alpha_{\rm crit}$ is not a good quantity to classify ELMs. In [9] it was concluded that the absolute value of the edge temperature may play a role in determining the ELM type. The temperature may influence MHD stability if resistivity plays a role. Then, a higher temperature stabilizes resistive modes and ideal effects dominate. We shall return to this when we discuss ELM models.

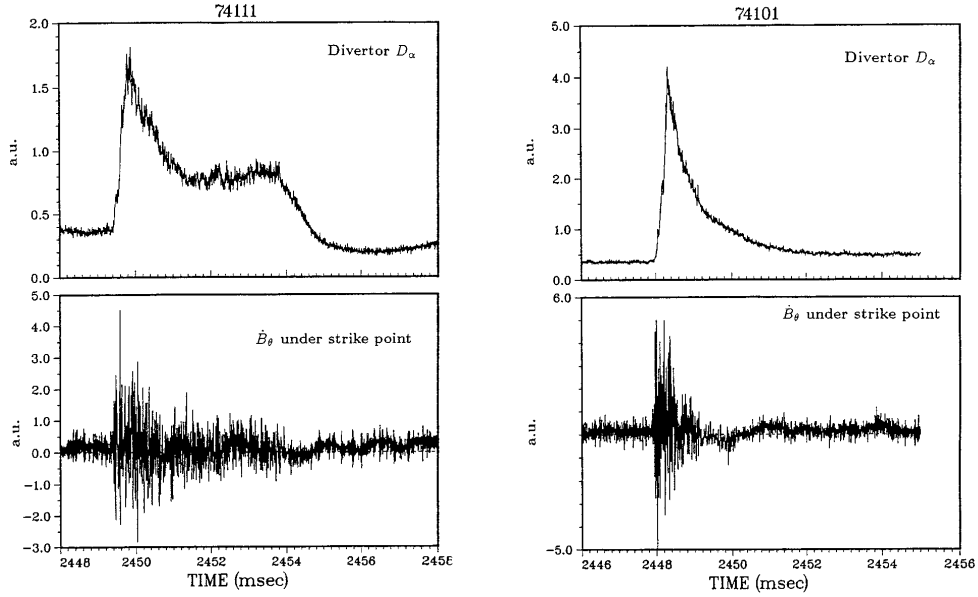

Figure 4. Comparison of a compound ELM (left) and a typical single type I ELM (right) on DIII-D. The compound ELM consists of an initial ELM, recognizable by the high level of magnetic fluctuations, and a subsequent L-phase.

In ASDEX, ELMs were always found to be MHD phenomena of duration $\leqslant$ 1 ms whereas in DIII-D, ELMs of duration up to $\approx$ 10 ms had been found. In [9], it is pointed out that these long events can be described as an initial MHD instability followed by a transient L-phase. This sequence has been dubbed 'compound ELM'. Figure 4 shows an example where the two events can be distinguished by their level of magnetic fluctuations. Obviously, the initial ELM event may lead to a decrease of $T_{\rm e}$ to a value below that necessary to sustain the H-mode. The subsequent reheating in the transient L-mode phase then leads to an L–H transition. It was concluded that ELMs are always MHD instabilities of duration $\leqslant$ 1 ms which, in a compound ELM, may be followed by a transient L-phase. On DIII-D, the initial ELM event can be either a type I or a type III ELM.

2.2.3. ASDEX Upgrade. In shape and size, the ASDEX Upgrade tokamak is comparable with DIII-D. Consequently, the phenomenology is very similar. In ASDEX Upgrade, type I and type III ELMs are clearly identifiable using the power dependence of the repetition

frequency. In addition, a magnetic precursor oscillation of frequency $\nu_{\mathrm{prec}} \approx 70$ kHz and poloidal mode number $m \approx 10$ is found prior to type III ELMs. Compound ELMs can be identified as an MHD event similar to a normal ELM followed by an L-phase lasting $\approx 5-10$ ms. However, no type II ELMs have yet been identified. One reason for this may be that the triangularity in standard ASDEX Upgrade discharges is much lower ($\delta \leqslant 0.1$) than that in the DIII-D discharges where type II ELMs occurred ($\delta \geqslant 0.4$). Although at present, no clear magnetic precursor oscillation prior to type I ELMs has been found in ASDEX Upgrade, there is a precursor oscillation on the edge electron temperature [15]. This is shown in figure 5, where a comparison of type III and type I precursors in ASDEX Upgrade is shown. The fact that this oscillation is not detected by magnetic probes points to either an electrostatic nature or a higher poloidal mode number than for the type III precursor.

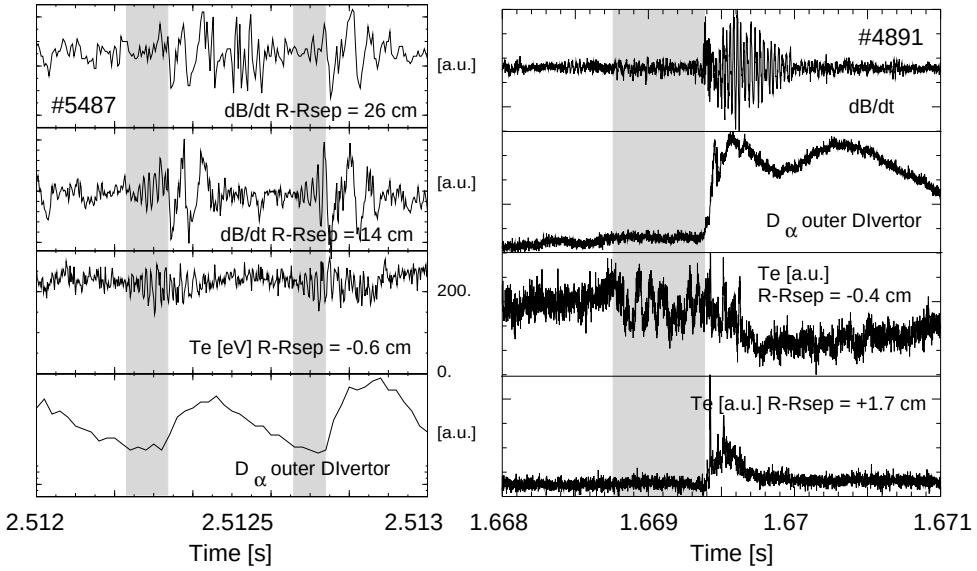

Figure 5. MHD signatures of type III (left) and type I (right) ELMs. The occurrence of a precursor is indicated by the shaded region.

In ASDEX Upgrade, modelling of the so-called dithering H-mode, a phenomenon first noticed in DIII-D [16], has been performed [17]. The dithering H-mode consists of a series of L–H–L transitions when the heating power is of the order of $P_{\mathrm{thr}}^{\mathrm{LH}}$ and can be modelled consistently by applying an H-mode model without using any MHD instabilities as a mechanism (see also section 3). Experimentally, type III ELMs, which also occur close to the threshold, can be distinguished from the dithering cycles by the occurrence of the magnetic precursor oscillation. In addition, as shown on ASDEX [13], during a type III ELM, the fluctuation level in both the magnetic field and the electron density reaches much higher values than in the temporary L-phase of a dither. However, during a power ramp-up, there is a gradual change from the first cycles that appear right at the transition which show no detectable precursor oscillation up to the last isolated type III ELMs before the ELM-free phase where clear precursor activity is seen. In between, the identification of the first type III ELM is somewhat arbitrary.

In ASDEX Upgrade, it was shown that the power dependence of the ELM frequency is governed by P_{sep}, the energy flux conducted through the separatrix, rather than by the

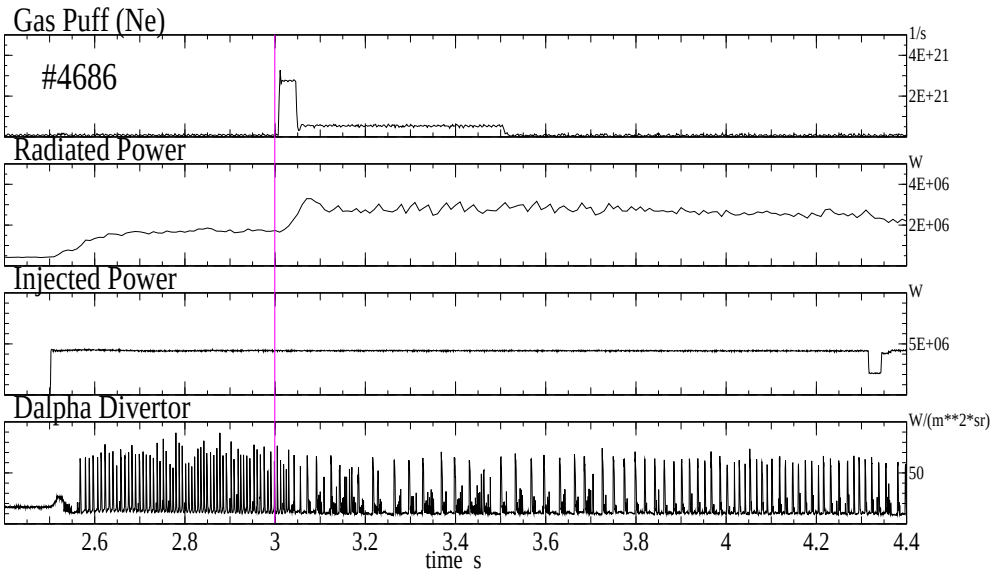

Figure 6. Variation of the ELM frequency with $P_{\rm sep}$ in ASDEX Upgrade. At constant P, $P_{\rm sep}$ is reduced by enhancing the radiative losses through injection of neon, leading to a decrease of the type I ELM frequency.

absolute value of the applied heating power. The sequence found during a power rise in DIII-D (see figure 2) is reversed if $P_{\rm sep}$ is reduced by enhancing the radiation losses from the plasma by injection of additional impurities. Figure 6 shows the variation of $P_{\rm sep}$ through injection of neon, leading to a decrease of the type I ELM frequency. A further increase of the radiated power leads to short ELM-free phases, followed by type III ELMs. Thus, at constant $P_{\rm tot}$, the ELM type and characteristic can be varied from the low-frequency type I ELMs to the high-frequency type III ELMs. Using this method, the amount of energy and particles expelled per ELM is greatly reduced and the effect of ELMs can be buffered in the divertor plasma. This so-called CDH-mode [18] may offer a solution to the power exhaust problem of the ELMy H-mode mentioned above.

An interesting observation is that in ASDEX Upgrade, without additional impurity puff, type III ELMs have so far only been observed in discharges with the favourable ion drift direction (towards the X-point). Note that, for the unfavourable direction, $P_{\rm thr}^{\rm LH}$ is higher by a factor of ≈ 1.8 [4]. For discharges with the same line-averaged density, $T_{\rm e}(a)$ is measured to be higher by a factor of ≈ 2 at the L–H transition for a discharge with the unfavourable drift direction. Again, this points to an influence of the absolute value of the edge temperature on the type III ELM stability. This is in fact supported by the observation that with additional radiative cooling via Ne injection, type III ELMs can also occur in discharges with the unfavourable direction.

2.2.4. Alcator C-MOD. The Alcator C-MOD tokamak ($R_0 = 0.67$ m, $a = 0.21$ m) is capable of producing an especially high toroidal field (up to 9 T) [19]. Thus, its parameter range is different from the other tokamaks discussed here. Nevertheless, H-modes are achieved and exhibit ELMs. So far, dithering cycles and type III ELMs have been obtained. Type III ELMs can be identified by their power dependence and the occurrence of a coherent

magnetic precursor oscillation. In Alcator C-MOD, an *in-situ* determination of 'local' poloidal and toroidal mode numbers is possible, i.e. from magnetic coils separated by small poloidal and toroidal angles, but not spanning the whole plasma circumference [20]. From these measurements, it is found that the frequency of the precursor ($\nu_{\mathrm{prec}} \approx 125$–$150$ kHz) and the poloidal mode number ($m \approx 8$–12) is well within the range of the other experiments. However, the inferred toroidal mode number of $n \approx 10$ is surprisingly high. It is, however, at the moment not clear whether this may be due to the fact that shaping and toroidicity steepen the local pitch of the field lines on the outside midplane to give a lower 'local' m or whether these findings indicate that the perturbation does not follow the equilibrium field lines.

2.2.5. COMPASS-D. The tokamak COMPASS-D has a shape similar to ASDEX Upgrade and DIII-D (elongated cross section with $\kappa \leqslant 1.7$), but is smaller (minor radius 0.17 m and major radius 0.56 m). Type III ELMs, characterized by the power dependence of the frequency and the magnetic precursor oscillation have been identified (called 'MHD-ELMs' on COMPASS-D [21]). In contrast, so-called L–H ELMs are distinguished. They appear at the L–H transition and are not single, isolated events, but rather a series of L–H–L transitions, thus bearing similarities to the dithering cycles. However, sometimes magnetic precursor activity is detected even between these events so that the clear distinction between type III ELMs and dithering cycles is not always possible.

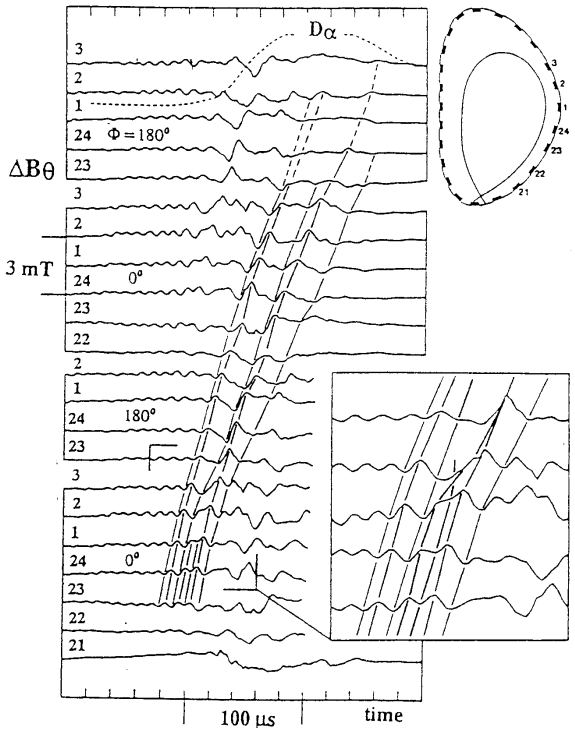

Figure 7. MHD mode structure of the type III ELM precursor inferred from magnetic measurements on COMPASS-D. At the onset of the ELM, there is an interchange of neighbouring flux bundles.

COMPASS-D is equipped with magnetic pick-up coils close to the plasma on the whole poloidal circumference. With these, it is possible to analyse in detail the structure of the type III ELM precursor [21]. Figure 7 shows such an analysis. The precursor structure (rotating at $\nu_{\mathrm{prec}} \approx 100$ kHz) can be traced around the poloidal circumference. A poloidal

mode number of $m \approx 13$ can be inferred. However, at the moment the actual ELM sets in, there is a defect in spatial periodicity which can be visualized as the interchange of poloidally neighbouring field lines carrying current filaments of opposite direction. During the event, the poloidal mode number roughly halves, leading to a wider radial extent of the perturbation. This interchange of neighbouring field lines on a flux surface can also be interpreted as the reconnection of magnetic flux, implying that resistivity plays a dominant role in the mechanism initiating the type III ELM.

On COMPASS-D, cases have been found where the magnetic precursor is scarcely detectable or does not grow explosively before the ELM event. Therefore, the role of the ELM precursor as the event initiating the ELM is not definitely clear on COMPASS-D. Recently, first hints of a magnetic precursor oscillation prior to type I ELMs were found in COMPASS-D [22]. In these cases, modelling of the measured magnetic signals as two chains of magnetic islands close to the separatrix led to stochasticity that was sufficient to explain the enhanced transport during the ELM.

2.2.6. JFT2-M. In the tokamak experiment JFT2-M ($R_0 = 1.31$ m, $a = 0.21$ m, $\kappa \leqslant 1.5$), ELMs have been characterized with respect to the power dependence of the repetition frequency [23]. It is found that ELMs occur at a heating power $P \approx P_{\rm thr}^{\rm LH}$ and become less frequent as P is increased until they are finally stabilized. From this characteristic it seems clear that in JFT2-M, type III ELMs are observed.

One interesting feature of the JFT-2M tokamak is the possibility of applying external magnetic field perturbations to ergodize the plasma edge. It is found that with a spectrum of high poloidal harmonics (m typically centered around 11), the stabilization of ELMs appears at higher heating power than without the resonant magnetic perturbations. It is interesting to note that application of these resonant magnetic perturbations also shifts $P_{\rm thr}^{\rm LH}$ to a higher value [24]; it seems that $P_{\rm sep} - P_{\rm thr}^{\rm LH}$ is the quantity that determines the type III ELM frequency. These observations could be consistent with recent COMPASS-D results, where the application of external magnetic field perturbations showed an increase of the type III ELM frequency at constant P [25]: if $P_{\rm thr}^{\rm LH}$ is increased by the resonant magnetic perturbations, this would reduce the effective heating power $P_{\rm sep} - P_{\rm thr}^{\rm LH}$.

2.2.7. JET. JET is the largest of the tokamak experiments ($R_0 = 3.1$ m, $a = 1.25$ m). The ELM phenomenology of JET shows clear differences between the different divertor configurations installed in the experiment. Up to 1994, discharges were mostly run in X-point configuration with the X-point close to the target plates. We shall refer to this configuration as the 'old' divertor. In 1994, a pumped divertor was installed allowing for a longer distance between X-point and target plates. Together with this, the plasma volume was decreased and the standard plasma shape was changed towards lower triangularity. This configuration will be referred to as the 'new' divertor. We shall discuss these two configurations separately.

With the old divertor, ELMs were usually observed close to the L–H threshold, their frequency decreasing with heating power. They were therefore identified as type III ELMs. It was shown that the ELM frequency has a strong inverse correlation with ∇p in the edge [26]. In detail, it was found that ∇n does not change significantly for different H-mode conditions whereas ∇T rises with an increase of heating power, again pointing to a significance of T or ∇T itself in addition to ∇p for the type III ELM behaviour. This is clearly seen in figure 8, where the arrival of sawtooth heat pulses in the edge increases $T_{\rm e}$ stepwise at more or less fixed ∇n and n and lowers the type III ELM frequency. This

means that, although the driving pressure gradient is increased by the rise in T_e, the type III ELMs are more stable; thus it points to a stabilizing role of T_e for type III ELMs. This will be discussed in detail in section 3.

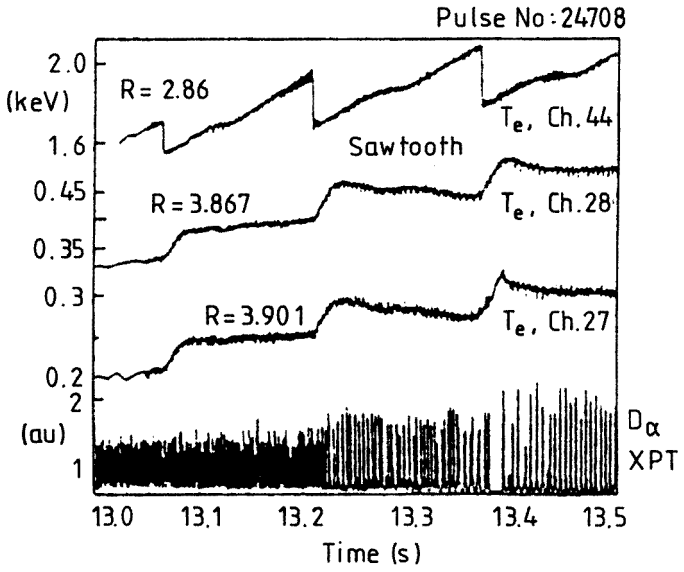

Figure 8. Change in the type III ELM frequency due to a change in the edge temperature by the arrival of sawtooth heat pulses in the edge plasma of JET.

Consistent with the classification as type III ELMs, magnetic precursor activity was found [27]. It consists of a coherent mode at frequency $\nu_{\text{prec}} = 80$–100 kHz. A toroidal mode number of $n = 8$–15 was inferred. The mode was not found to grow dramatically in amplitude before the ELM. However, the actual ELM, seen as a broadband turbulent event, usually leads to the disappearance of the mode. Thus, a causal relationship between the magnetic oscillation and the ELM seems to exist.

Analogously to DIII-D results, an ideal ballooning analysis reveals that during type III ELMs, the edge pressure gradient is far from the ideal ballooning limit (typically $\alpha \leqslant 0.3\alpha_{\text{crit}}$) [28]. There are also cases where, in the old JET, the edge pressure gradient was found to be close to the ideal ballooning limit; it is suspected that in these cases (e.g. high β_p H-mode [29]), the ELMs are of type I. However, the power dependence of ν_{ELM} in these discharges is not reported.

In contrast to the old JET configuration, where type III was the most common ELM type, in the new JET configuration, mainly type I ELMs, identified by their increasing repetition frequency with increasing heating power, are observed. It is at the moment not clear, where this change comes from. However, as previously mentioned, with the new divertor the plasma shape and size were appreciably changed compared with the old discharges.

During experiments aimed at establishing long ELM-free phases, it was again found that, analogously to DIII-D, an increase in triangularity suppresses onset of the ELMs both with the old divertor [30] and with the new divertor [31]. Ideal ballooning analysis again shows that the effect of high triangularity is to move the plasma edge into the second stable region.

With the new configuration, it has been found that in some cases, ELMs may have a

more severe effect on energy confinement than in others. Spatially resolved measurements of T_e show that in some cases, T_e drops even inside $a/2$ within a few ms after the ELM event. A transport analysis indicates that χ has to be enhanced in the outer plasma region to a high value and, in addition, χ has to be switched to the L-mode value in the whole plasma [32]. This observation, which seems to contradict the edge localization of the ELM, may be resolved by the fact that these events last longer than the usual ELMs: they can be identified as compound ELMs. In this interpretation, the enhanced χ in the outer plasma region is due to the effect of the ELM as an MHD phenomenon. In the subsequent L-phase, the transport is on L-mode level in the whole plasma. This is consistent with recent results where it is shown that, in JET, the L–H transition happens on a fast timescale on the whole plasma radius [33]. Thus, the temporal behaviour of T_e during compound ELMs proves that the H–L transition is also a global event that propagates to the core plasma much faster than on the diffusive timescale.

2.2.8. PBX-M. The PBX-M tokamak ($R_0 = 1.65$ m, $a = 0.3$ m) runs highly shaped plasmas ($\kappa \approx 1.9$, indentation on the high field side). In H-mode discharges, ELMs occur. However, the classification of the different phenomena is not entirely clear. In experiments at relatively low β, where single ELMs occurred, it was found that no coherent magnetic precursor oscillation could be detected, but there was a pronounced change in the correlation of magnetic fluctuations: prior to the ELM, the correlation in the high-frequency range ($\nu \geqslant 250$ kHz) increases [34]. Then, at the onset of the ELM (defined by the D_α-rise), an increase in coherence at $\nu \approx 200$ kHz is found.

During the ELM itself, the coherent magnetic fluctuations can be interpreted as composed of mode structures ranging from $n = 3$ to $n = 8$. The coherence of the fluctuations only showed the distinct increase on the outside midplane; thus, an outward ballooning character of the mode structure was deduced. This is consistent with the interpretation of the structures as kinetic ballooning mode.

In experiments at high β, a magnetic precursor oscillation with inward ballooning character was detected. It was concluded that this behaviour contradicts the ideal ballooning mode, but is consistent with ideal kink calculations [35].

2.2.9. TCV. The TCV tokamak ($R_0 = 0.88$ m, $a = 0.25$ m) is designed to run a variety of different shapes of the poloidal cross section. Thus, the influence of plasma shape on ELMs can be studied. First results from TCV, all of them obtained in ohmic H-mode, indicate the occurrence of dithering cycles at the L–H transition and type III ELMs [36]. However, type I ELMs have not yet been uniquely identified. In addition, edge localized fluctuations have been detected that do not significantly affect confinement but are seen on the D_α-signal. These have been dubbed 'mossy ELMs' and their interpretation is not yet clear.

In TCV, ELM control experiments have been carried out by dynamically varying the configuration [37]. For this purpose, a double-null discharge is run that is slightly imbalanced so that, for preference, one X-point is active. Thus, the active X-point can be switched by small changes in the equilibrium. In this method, it is mainly the relative orientation of the ion ∇B drift and the active X-point that are varied. It is found that, at a given heating power, with the ion ∇B drift towards the X-point (favourable drift direction), the discharge is ELM free, whereas with the other orientation, ELMs prevail. Although not uniquely identified, these ELMs are probably of type III (low heating power, high repetition frequency). Then, the result can be interpreted analogously to the JFT2-M and COMPASS-

D experiments using resonant magnetic perturbations. As pointed out above, the power threshold for the L-H transition is higher in the unfavourable direction. As discussed for JFT2-M, the type III ELM behaviour seems to be governed by $P_{\rm tot} - P_{\rm thr}$ rather than by $P_{\rm tot}$. Thus, in the unfavourable direction, type III ELMs occur (close to the threshold), whereas for the favourable direction, $P_{\rm tot} - P_{\rm thr}$ is higher and type III ELMs are already suppressed.

2.2.10. Wendelstein VII-AS. In H-mode discharges in the stellarator WVII-AS, short bursts in the D_α-light associated with an edge instability are observed. They are identified as ELMs [38]. However, a classification by the criteria applied to the tokamak experiments described above has not yet been made. The power dependence of $\nu_{\rm ELM}$ is not yet clear, mainly because ELMs up to now appear as irregular bursts. A magnetic precursor has not yet been found; however, its existence cannot be ruled out on the basis of the experimental results known at present.

WVII-AS differs appreciably from the tokamaks described above. It has a high aspect ratio ($R_0 = 2.0$ m, $a \approx 0.17$ m). The other major difference is that there is no net toroidal current. It should be mentioned that in the edge region, the pressure gradient drives a bootstrap current. A role of this current in determining ELM physics cannot be ruled out [38], although it changes the safety factor by $\leqslant 1\%$. This points to a dominant role of the edge pressure gradient rather than the toroidal current as the driving mechanism for the ELMs occurring in WVII-AS.

2.3. General classification

From these various experimental observations, we propose to classify ELMs according to the occurrence of the magnetic precursor and the dependence of the ELM frequency on the energy flux through the separatrix, $P_{\rm sep}$. As has been shown above, ideal ballooning stability is not a good criterion for separating the different ELM types. Moreover, the shape and magnitude of the D_α-signal in the divertor will not be used to identify a specific ELM type. Finally, we shall also omit type II ELMs, because at present, they have only been found in special DIII-D discharges. Instead, we add the dithering cycle as an edge localized phenomenon. We arrive at the following definition

- *Type I ELMs*. The ELM repetition frequency $\nu_{\rm ELM}$ increases with the energy flux through the separatrix:

$$\frac{{\rm d}\nu_{\rm ELM}}{{\rm d}P_{\rm sep}} > 0. \tag{2}$$

  At present, no clear coherent magnetic precursor oscillation has been identified, although indications for a precursor oscillation of $T_{\rm e}$ and, in some cases, for magnetic precursors exist. It is not clear whether the absence of a magnetic precursor oscillation is due to a lack of diagnostics. Prior to type I ELMs, the overall fluctuation level increases. During the ELM, there is a high level of incoherent magnetic fluctuations.
- *Type III ELMs*. The ELM repetition frequency decreases with the energy flux through the separatrix:

$$\frac{{\rm d}\nu_{\rm ELM}}{{\rm d}P_{\rm sep}} < 0. \tag{3}$$

  The type III ELM frequency is characterized by the heating power in excess of the power threshold, i.e. $P_{\rm tot} - P_{\rm thr}$. A coherent magnetic precursor oscillation of toroidal mode number $n \approx 5$–10 and poloidal mode number $m \approx 10$–15 is observed on magnetic

probes located close to the plasma, especially in the outboard midplane. During the ELM, there is a high level of magnetic fluctuations.

- *Dithering cycles*. For $P_{\rm sep} \approx P_{\rm thr}^{\rm LH}$, repetitive L–H–L transitions may occur. The repetition frequency shows a slight decrease with increasing $P_{\rm sep}$. Dithering cycles show no magnetic precursor oscillation; the level of turbulence during the temporary L-phase does not significantly exceed that of the L-phase at $P_{\rm sep} \leqslant P_{\rm thr}^{\rm LH}$.

Here, the occurrence of the different ELM types has been described in terms of tokamak operational parameters, i.e. heating power etc. For a physical description, a description in terms of the plasma parameters such as T and n would be desirable. However, due to the steep edge gradients and their fast temporal variation, this information will in general only be available in future experimental investigations with improved diagnostics. This will clarify some of the physical aspects, such as the role of $T_{\rm e}$ in the type III ELM behaviour.

For both type I and type III, the ELM itself is an MHD event lasting 0.3–1 ms. In particular, the duration does not seem to vary significantly with the machine size (e.g. JFT-2M and JET report a duration $\geqslant 0.5$ ms, although their minor radii vary by a factor of $1.25/0.21 \approx 6$). However, so-called compound ELMs, i.e. ELMs with a subsequent L-phase of 5–15 ms duration have been identified on various experiments. Typical type III repetition frequencies are in the 2 kHz range (i.e. frequency of the order of the inverse of the duration) down to 200 Hz in steady state ELMy H-mode discharges. Typical type I ELM repetition frequencies are reported in the range 10–200 Hz. However, for the lowest ELM frequencies, when the inverse of the ELM frequency is of the order of the confinement time, it remains a matter of definition whether one speaks of 'ELM-free phases' between the single ELMs.

From the previous discussion, it is clear that the classification is valid for all tokamak experiments analysed above.

2.4. ELM effects on transport

It was shown above that an ELM leads to a loss of energy and particles from the plasma edge. For a detailed discussion, we refer to a recent paper [39], the main results of which will be summarized here.

ELMs degrade the global particle and energy confinement time. However, as only the edge region is affected by the ELM transport, the reduction is much more severe for the particle confinement, as the loss region equals the source region, whereas for the energy, only the part of the (centrally deposited) energy that has been transported into the edge region, is affected. Thus, ELMs provide density control for only a modest reduction of $\tau_{\rm E}$.

It is found that individual ELMs decrease the plasma energy and particle content by roughly 5–10%. There is a tendency for the effect of type III ELMs to increase with decreasing ELM frequency whereas, at least at high heating power, when the ELM duration is roughly constant, the absolute value of the energy loss per type I ELM is nearly constant. In contrast, ELMs that last for longer times (so-called 'compound ELMs', see below) may have a more severe effect on the stored energy and particles. These results will have to be examined in a more systematic manner to yield predictions for future machines such as ITER. The analysis also shows that during ELMs, high heat and particle fluxes may occur that may lead to unacceptable loads on the target plates in a reactor. Thus, tailoring of ELM type and frequency may be necessary in a reactor.

3. ELM Models

We shall now review existing ELM models and their relation to the experimental findings. Often, it is not explicitly stated which ELM type the model should describe; in these cases, we shall try to determine the ELM type potentially described by the model. Two basic models exist. One is the description of ELMs as a limit cycle oscillation at the L–H threshold. In the other one, if additional physics such as a stability limit is considered, a limit cycle occurs at higher heating power. These models do generally not describe the detailed physics of the ELM process. The other class of models uses MHD stability analysis to find MHD modes that become unstable at the ELM onset. We shall discuss the two classes of models separately and then relate them to the experimental findings.

3.1. ELMs as Limit Cycle Oscillations

It was mentioned above that, due to the hysteresis of the L–H power threshold, a limit cycle oscillation at the power threshold may occur. The original scope of the bifurcation model used to describe the dithering cycles [17] was the explanation for type III ELMs in JFT2-M [40]. It was concluded that the limit cycle oscillation found at the L–H threshold might be a description of type III ELMs. In a recent update of the theory [41], it was shown that an increased outflux of particles, for example due to an MHD instability associated with a type I ELM, can trigger a transition back to the L-mode followed by an L–H transition. While this model might correctly describe the sequence observed during compound ELMs, it does not give an explicit calculation for the type I ELM itself (the first increase in outflux was artificially prescribed in the model).

Several possible limit cycle oscillations are also found by other authors treating the temporal behaviour of the L–H transition. One example is the theory developed by Diamond *et al* [42]. Here, radially averaged equations for the temporal evolution of the amplitude of the turbulent fluctuations and the poloidal rotation are derived. The poloidal rotation is determined by the torque due to Reynold's stress, i.e. non-ambipolar anomalous transport and the dissipation due to magnetic pumping. The amplitude of the turbulent fluctuations is reduced by radial shear in the poloidal flow. In this system, it is found that at the L–H transition, dithering cycles may occur. If further physics is incorporated in the equations, other limit cycles can be identified. In [43], the ideal ballooning limit was heuristically incorporated to limit ∇p. In this case, periods of enhanced transport occur. Their repetition frequency increases with the energy flux through the system, thus, they are identified as type I ELMs. If instabilities associated with the rotational dynamics of the plasma edge (such as the Kelvin Helmholtz instability), are incorporated into the model, another limit cycle is found. Here, the edge pressure gradient may be below the ideal ballooning limit, but the rotational instability leads to increased transport. It is found that this instability becomes less frequent with increasing energy flux, hence, it is identified as a type III ELM.

Another system describing the dynamics of the L-H transition was developed by Sugama and Horton [44]. Here, three radially averaged equations are derived to describe the temporal evolution of the plasma edge pressure gradient, the amplitude of pressure-driven resistive turbulence and the poloidal flow velocity. Again, a limit cycle oscillation is found, not at the level of energy flux required for the L–H transition, but at higher energy flux. Consequently, this model should describe ELMs rather than dithering cycles. The authors conclude that their model describes type III ELMs, in contrast to the dithering cycles described by the model used by Itoh *et al* [40] and Zohm [17].

Finally, a limit cycle between electrostatic and magnetic turbulence (so-called M-mode)

has been proposed by Itoh *et al* [45]. It is shown that at low pressure gradients, electrostatic fluctuations prevail whereas at high pressure gradients, magnetic islands can overlap and thus, stochasticity evolves. It is found that there is a critical value of the pressure gradient at which this switch from L-mode to M-mode occurs. Although obtained from a nonlinear, saturated turbulence calculation, the critical gradient is close to that given by the linear stability boundary obtained by ideal ballooning analysis.

3.2. ELMs as MHD instabilities

Several authors have performed detailed MHD stability analyses of experimental and theoretically specified pressure and current profiles to decide whether they are unstable to a specific MHD instability. However, the usual linear stability analysis indicates whether or not a mode will initially grow, but it cannot predict the actual effect of the mode on transport. This has to be inferred from nonlinear stability analysis which indicates the level of perturbation at which a mode will saturate. Then, the effect of the saturated mode, or the combined effect of several interacting modes, on confinement has to be estimated. The nonlinear part of the MHD stability analysis is usually difficult to compute and thus, usually, theoretical estimates of the ELM effect on transport are not given.

The first MHD stability analysis to infer the ELM mechanism was performed by Gohil *et al* [7]. An infinite-n ideal ballooning analysis was performed for DIII-D discharges exhibiting type I ELMs (at that time called 'giant ELMs'). It was found that the edge pressure gradient always builds up until the critical value $\alpha \approx \alpha_{\mathrm{crit}}$ is reached. Then, a type I ELM occurs. This is a result of linear stability analysis; the authors do not propose an explicit model to describe how the ballooning mode itself leads to the rapid transport of plasma across the separatrix. This can be described by a so-called 'avalanche model', which shows that the onset of ideal ballooning modes at one point steepens the pressure gradient in the vicinity and leads to an 'avalanche' of ideal ballooning modes, propagating radially faster than the diffusion timescale [46].

A different kind of analysis was carried out by Kerner *et al* for ASDEX, i.e. for type III ELMs (reported in [14]). Here, a nonlinear calculation in cylindrical geometry with a free boundary was performed. It was found that for sufficiently strong gradients of the edge current density and pressure, a nonlinear turbulent mixture of resistive interchange modes can couple to a kink instability, leading to rapid ($\approx 20\ \mu$s) destruction of the outer flux surfaces of the plasma ('peeling mode'). In this model, the driving forces for the type III ELM are both the current and the pressure gradient in the edge. An example of a 'peeling off' of flux surfaces is shown in figure 9.

An extension of this type of model was given by Huysmans *et al* for JET type III ELMs [47]. Here, a linear stability analysis with free boundary taking into account the effects of toroidicity and shape of the plasma cross section was performed. Resistive ballooning modes (as an analogue to the resistive interchange in toroidal geometry) were found to be unstable for high mode numbers ($n \geqslant 10$). As these modes are radially very localized and have a slow growth rate, it was concluded that they might explain the observation of the type III ELM precursor oscillation; however, they cannot explain the type III ELM mechanism itself. It was suggested that the resistive ballooning activity leads to a steepening of the edge pressure and current profiles and then couples to a lower-n free boundary mode, to form a peeling mode. Linear free boundary tearing mode analysis showed that for JET model profiles, the growth rate (10^4 times the Alfven time, which itself is of the order of some μs) was too slow to explain the rapid growth at the onset of the ELM. However, by increasing the edge current density or the resistivity, the authors found that the growth

time could be of the order of 10–100 times the Alfven time, which might explain the ELM onset. It was shown that the edge current density gradient is the main driving force of this instability. For $n > 1$, the pressure gradient also enters as a destabilizing force. However, a nonlinear calculation showing the coupling of the several modes has not yet been performed for this model.

A possible role of the external kink mode for the ELM mechanism was also stressed by Manickam [48]. Here, the linear stability of the external kink mode is studied for a variety of current and pressure profiles in the ideal case, i.e. neglecting plasma resistivity. It is found that the stability is determined by the stabilizing effect of the edge shear and the edge current density as the main driving forces. Thus, analogously to the discussion given above, a build up of the edge current density tends to drive the external kink unstable. This is even true if the analysis is performed for a pressureless plasma. Introducing a finite pressure gradient, it is found that the mode can either have the structure of a peeling mode, i.e. edge localized, or couple to the plasma interior thus extending over a wider radial zone. It is concluded that the ideal kink might be a candidate for the type I ELM mechanism

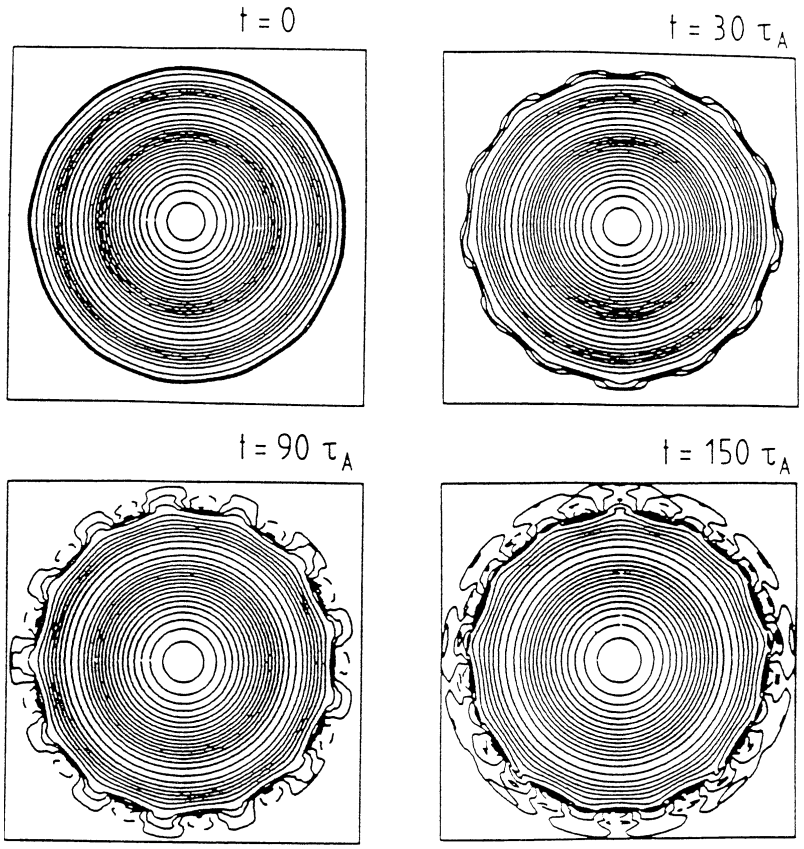

Figure 9. Peeling mode in cylindrical geometry leading to a rapid loss of plasma across the boundary. The plot shows the temporal evolution of the plasma pressure. This type of mode was suggested as the type III ELM mechanism on ASDEX.

(called 'giant ELM' by the author). In particular, it is stated that the short growth times observed in the experiment ($\approx 10\ \mu$s) are consistent with the ideal external kink. However, no specific comparison with actual experimental profiles is made. Furthermore, the question of how the enhanced transport of plasma during the ELM happens is not addressed.

4. Discussion

Based on the discussion of the experimental findings and the theoretical models, we now try to establish a physical picture of the different ELM phenomena. As shown above, the ELM models generally give no quantitative description of how energy and particles are lost during the ELM; thus, a comparison with the experimentally determined transport properties of ELMs cannot be made. However, we can compare with the experimentally observed timescales, i.e. the rise time of the ELM, the duration and the behaviour of the ELM repetition frequency. In addition, the radial extent of the mode should be given by theory and can be compared with the experimental findings.

It was shown above, that time-dependent models of the L–H transition can exhibit dithering cycles, i.e. series of L–H–L transitions. This is consistent with the experimental picture that dithering cycles are not primarily MHD events (no precursor, low fluctuation level). It was shown that for the model of Itoh *et al*, the repetition frequency of the dithering cycles is given by the diffusion time in the transport barrier, yielding a timescale consistent with the experiment [17]. The radially averaged model of Diamond *et al* does not give quantitative predictions about the timescale of the cycle; this should be addressed in further work. Thus, the physical picture of the dithering cycles is that of a limit cycle oscillation associated with the hysteresis in the L–H transition. As has been shown above, the dithering cycles only affect temperature and density in the transport barrier. Thus, type III ELM models which require sufficient gradients of the edge pressure and current density are not applicable to the dithering cycles right at the transition.

Type III ELMs differ from the dithering cycles in that they exhibit strong MHD activity. The actual transport during a type III ELM can be much higher than in an intermediate L-phase. Therefore, an MHD instability must be identified as the type III ELM mechanism. DIII-D and JET show that type III ELMs may occur well below the ideal ballooning limit. Therefore, this instability can be ruled out as a possible candidate.

The time-dependent, radially averaged H-mode models by Diamond *et al* and Sugama *et al* both find a limit cycle not associated with the L–H transition itself. In the case of Sugama *et al*, this is a natural consequence of the system of equations treated there. In this picture, the type III ELMs are assumed to correspond to bursts of resistive pressure-gradient-driven instabilities which might explain the high magnetic turbulence level observed during the type III ELM. The variation of the ELM repetition frequency with input power ($\mathrm{d}\nu_{\mathrm{ELM}}/\mathrm{d}P < 0$) is also consistent with the experimental behaviour of type III ELMs. However, as the model is radially averaged, no definite statement about the timescale of the ELM itself is made. Finally, the model does not predict the occurrence of a coherent magnetic precursor oscillation. This oscillation must be interpreted as a single mode rather than turbulence, which gives rise to incoherent fluctuations of the magnetic field. Thus, at the moment, the model can only be regarded as an idealized description of a limit cycle representative for type III ELMs.

The same criticism holds for the type III ELM limit cycle presented by Diamond *et al*. It does not appear in the original system of equations describing the dynamics of the L–H transition, but is a consequence of the addition of terms describing a rotational instability associated with the free energy available from the sheared flow. While it is stated that

the frequency of this repetitive instability decreases with heating power (which would be correct for type III ELMs), there is no statement about the actual timescales involved in the process. Moreover, no prediction of the spatial structure (precursor, fluctuation spectra etc) of the instability is currently given by the model.

The MHD models by Kerner *et al* and Huysmans *et al* yields more details about the MHD structure of the type III ELM. However, the identification of resistive ballooning modes with $n > 10$ as the ELM precursor as given by Huysmans *et al* does not really match the experimental finding of a single mode with $n \leqslant 10$. The ELM mechanism itself, a peeling mode coupled to turbulent fluctuations, has been shown to have the right growth time of the order of several tens of μs. The role of the increased edge current density gradient required to drive the mode unstable may be consistent with the experimental observations; it is generally observed that during the H-mode, the internal inductivity of the plasma decreases, indicating a broadening of the current density profile. In the future, an interesting contribution to this field may be made by stellarators, which exhibit only a small edge current.

Both the MHD model and the limit cycle discussed by Sugama *et al* interpret the ELM as a resistive phenomenon. This is consistent with the experimental fact that the edge temperature plays a crucial role in the type III ELM behaviour. All experimental evidence discussed above shows the tendency for a higher edge temperature to stabilize type III ELMs. This might also be the explanation for the frequency dependence of type III ELMs; the time interval between two ELMs is governed by the time it takes to build up the pressure and the current density gradients until the stability limit is reached. For a resistive instability, a rise in T due to a rise in heating power will shift the stability boundary to higher values, and increase the time it takes to develop the critical gradients. This is consistent with the observation shown in figure 8 where $T_e(a)$ is increased in steps and the type III ELM frequency decreases. Obviously, the driving term due to the increase in ∇p when ∇T is increased is overcome by the stabilization due to the higher absolute value of T_e. This dependence would also explain the fact that the energy loss per type III ELM increases with decreasing frequency: at higher T_e, a higher edge pressure gradient has been built up; the release of energy due to the ELM can therefore be higher. In addition, as shown above (figure 7), the growth of the coherent precursor mode and the event initiating the ELM might be linked to a reconnection of magnetic flux, which is typical for a resistive phenomenon. Figure 10 gives a sketch of the physical picture of the type III ELM.

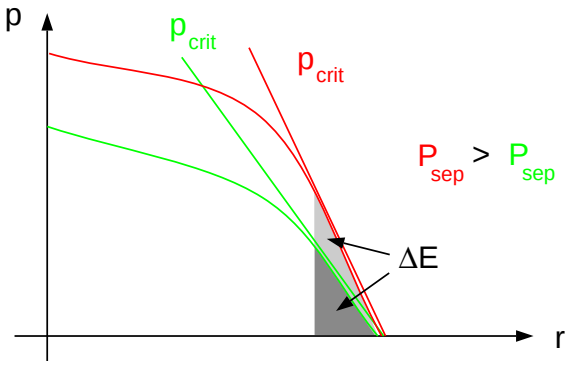

Figure 10. Sketch of type III ELM stability. The stability boundary increases with heating; thus, a higher ∇p develops before the ELM. Consequently, ν_{ELM} decreases and ΔE increases with power.

The situation is different for type I ELMs. Here, with the present diagnostics, no clear magnetic precursor can be detected. However, as pointed out above, various hints for

increased fluctuation level prior to type I ELMs as well as hints for precursor oscillations in T_e, and, to a limited extent, also in the magnetic field, may point to a precursor activity that can scarcely be detected with present diagnostics. This in turn implies a higher poloidal mode number of the modes involved. Furthermore, it was shown that the type I ELM itself is a rapid event and happens at higher temperature than the type III ELM, so that it might be linked to an ideal MHD phenomenon. This is consistent with the ideal ballooning analysis which shows that, on JET and DIII-D, the edge pressure gradient reaches $\alpha \approx \alpha_{crit}$ prior to a type I ELM. This would also explain the frequency dependence of type I ELMs: unlike for type III ELMs, the stability boundary is fixed to a large extent by the geometry of the flux surfaces even if the absolute value of T varies. Thus, a higher heating power that leads to a faster build up of the edge pressure gradient results in a higher ELM frequency. Note that, as the stability boundary does not vary with heating power, the edge pressure gradient does not change significantly. This might explain why, unlike for type III ELMs, the energy loss per type I ELM does not vary significantly with heating power in cases with high ELM frequency. A sketch of the physical picture of type I ELMs is given in figure 11.

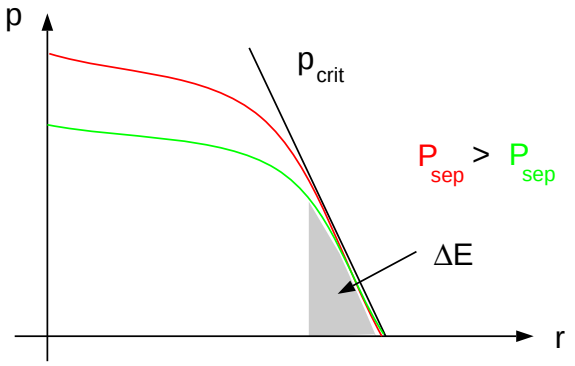

Figure 11. Sketch of type I ELM stability. The stability boundary is fixed, hence, ν_{ELM} rises with heating power and ΔE is roughly constant.

Further experimental evidence in favour of the ideal ballooning mode as a possible type I ELM mechanism is the fact that in cases where type I ELMs are suppressed, stability analysis often finds that the plasma edge has access to the second stable region of the ideal ballooning diagram. This is especially true for scenarios where strong shaping is applied and long ELM-free phases are observed at high heating power, such as in the VH mode in DIII-D [11] or JET [30].

Somewhat in conflict with the interpretation of the type I ELM as an ideal ballooning mode is the experimental observation that in DIII-D, the edge pressure gradient may reach the ideal ballooning limit and be at this value for several 100 ms without an ELM happening. In this sense, the condition $\alpha \approx \alpha_{crit}$ may be necessary but not sufficient for a type I ELM. An example for this is the occurrence of type III ELMs even at the ballooning limit in small devices with circular cross section, i.e. ASDEX and the ASDEX-like plasmas in DIII-D. Moreover, as discussed above, no actual model exists that explains how high-n ideal ballooning modes can enhance transport to the level observed during an ELM. One might therefore speculate that the ideal ballooning limit clamps the pressure gradient to $\alpha \approx \alpha_{crit}$, but the actual type I ELM happens through coupling of the ideal ballooning mode to another instability. An indication for the existence of another type of instability involved in the type I ELM is also given by the power deposition pattern on the divertor plates during type I ELMs. As mentioned above, type I ELMs deposit a large energy flux on the inner target plate, whereas for ballooning modes, where the amplitude of the perturbation is high

on the low field side, one might expect the power deposition to be mostly on the outer target plate. This other instability might be of the type of an external kink as discussed by Manickam. If a lower-n MHD instability is involved in the process, the 'peeling off' of flux surfaces might explain the very rapid transport during the ELM. Reconstructions of DIII-D equilibria prior to type I ELMs showed indications for a non-zero current density at the plasma edge [9], which is the main driver for an external kink. As shown above, type I ELMs change the edge current density, thus potentially reducing the driving force of the edge current density gradient. However, the role of an ideal kink in type I ELMs has not yet been verified experimentally. One exception to this is the termination of the long ELM-free phase in a VH-mode in DIII-D: there, the terminating event clearly has a low-n component consistent with a kink instability [11]. Finally, it should be noted that none of the ideal ballooning calculations mentioned above treats the effect of sheared flow on the ballooning stability; thus, at least in the transport barrier itself, the analysis should be treated with caution.

A different explanation for type I ELMs might be the switch from electrostatic to magnetic turbulence as discussed in the model of the M-mode [45]. As mentioned above, the stability boundary for type I ELMs as estimated from this model is close to the ideal ballooning limit, thus correctly describing the experiments. In addition, a hysteresis between the switch back and forth exists. This can explain why, when the stability boundary is reached, ELMs happen as distinct separate events and do not just continuously maintain the pressure gradient at that level. Thus, the model offers a potential description of type I ELMs; however at present, a more quantitative check against the experiments has to be performed.

Thus, we propose the following physical picture of the different ELM phenomena:

- *Dithering cycles*. At the L–H transition, a limit cycle oscillation due to the hysteresis of the H-mode power threshold may occur. The edge pressure and current gradients are close to their L-mode values, hence, the dithering cycles are not specific MHD instabilities, but L–H–L sequences.
- *Type III ELMs*. After the L–H transition, steeper gradients of the edge pressure and current density develop due to the edge transport barrier. They are sources of free energy for resistive MHD instabilities provided T_e in the edge is not too high. These instabilities are the type III ELMs, potentially a complex coupled MHD phenomenon consisting of high-n resistive instabilities such as resistive ballooning modes and a low-n kink-like free boundary instability that may rapidly enhance transport due to 'peeling off' of flux surfaces. An increase in edge temperature tends to shift the stability boundary for the resistive modes to higher values of pressure and current gradient, resulting in a decrease of the ELM repetition frequency with input power. For sufficiently high temperature, resistive effects no longer play a role and type III ELMs are suppressed.
- *Type I ELMs*. At high edge temperature, when type III ELMs are suppressed, the ideal ballooning mode limits the achievable edge pressure gradient to $\alpha \approx \alpha_{crit}$. If the ideal ballooning modes couple to a low-n instability (potentially again a kink-like instability due to the high edge current density), a type I ELM develops. If, through plasma shaping, the plasma edge has access to the second stability regime of ballooning modes, the type I ELM is suppressed and the limit to the edge pressure gradient is given by the occurrence of low-n MHD instabilities.

It should be noted that this physical picture cannot yet be taken as a definite description of the complex nonlinear physics of the ELM; however, it matches the experimental observations and is based on the fundamental physics identified by MHD stability analysis.

More is required on both the experimental and the theoretical side to validate the ideas expressed above.

5. Summary and conclusions

ELMs are MHD instabilities driven by the steep gradients of edge temperature and density in H-mode plasmas. They expel energy and particles from the plasma edge. The important role of ELMs is to provide stationary H-mode discharges (ELMy H-mode) when repetitive ELMs occur and help to control the particle inventory of the plasma. From the variety of edge localized phenomena occurring in toroidal fusion plasmas, three distinct types can be classified.

Dithering cycles. Due to the bifurcated character of the H-mode, at $P_{\mathrm{sep}} \approx P_{\mathrm{thr}}^{\mathrm{LH}}$, repetitive L–H–L transitions can occur. Dithering cycles show no magnetic precursor oscillation; the level of turbulence during the temporary L-phase does not significantly exceed that of the L-phase at $P_{\mathrm{sep}} \leqslant P_{\mathrm{thr}}^{\mathrm{LH}}$.

Type III ELMs. The ELM repetition frequency decreases with the energy flux through the separatrix in excess of P_{thr}, i.e. $\mathrm{d}\nu_{\mathrm{ELM}}/\mathrm{d}P_{\mathrm{sep}} < 0$. A coherent magnetic precursor oscillation with toroidal mode number $n \approx 5$–10 and poloidal mode number $m \approx 10$–15 is observed on magnetic probes located close to the plasma. During the ELM, there is a high level of magnetic fluctuations. Type III ELMs are stabilized at high edge temperatures, indicating that they are connected with resistive MHD instabilities. Candidates for the type III ELM mechanism include resistive ballooning modes, coupled to a global instability such as the free boundary mode ('peeling mode').

Type I ELMs. The ELM repetition frequency ν_{ELM} increases with the energy flux through the separatrix, i.e. $\mathrm{d}\nu_{\mathrm{ELM}}/\mathrm{d}P_{\mathrm{sep}} > 0$. In present experiments, no clear coherent magnetic precursor oscillation has yet been detected; during the ELM, there is a high level of incoherent magnetic fluctuations. The lack of a magnetic precursor may be due to a lack of diagnostics able to detect MHD modes of high mode numbers which in turn might indicate that type I precursor activity has even higher mode numbers than type III precursors. The power dependence and results from magnetic stability analysis indicate that type I ELMs are linked to ideal MHD instabilities. Type I ELMs may be stabilized by opening access of the plasma edge to the second stable ballooning region. However, the ideal ballooning criterion seems to be a necessary but not sufficient condition for a type I ELM. A plausible candidate for type I ELMs is therefore a combination of ideal ballooning modes coupled to a global ideal MHD instability such as an ideal kink.

The description of ELMs is still qualitative. Obviously, a linear stability analysis of typical current and pressure profiles can give an indication about the unstable MHD modes. However, theoretical ELM studies have to face the need for nonlinear calculations that actually describe the enhanced transport during the ELM. In general, this leads to a huge computational effort, but seems to be feasible in the future. In addition, the radial extent of the MHD modes leading to ELMs can be quantified by model calculations and then compared with the experimental results.

In the experiment, a better quantitative characterization of the stability boundaries of the different ELM types seems to be possible in the near future. This is due to the ongoing improvement in diagnostics that determine the profiles of temperature, particle density and current density with high spatial and temporal resolution. These profiles may serve as input for the theoretical analysis.

Finally, there is a lack of magnetic mode analysis during the ELM itself. The theoretical models described in this work predict that global MHD modes of low toroidal mode number

are involved in the ELM mechanism itself. However, their characteristics may be difficult to extract from measurements of the fluctuating magnetic field due to the overlaid broad-band turbulence from small-scale fluctuations during the ELM. The identification of global MHD modes involved in the ELM process remains a challenge for further experimental investigations.

Acknowledgments

I should like to thank my colleagues at different fusion laboratories for providing experimental data and for stimulating discussions that led to the preparation of this article. Special thanks are due to Dr H J de Blank for carefully reading and discussing the manuscript.

References

[1] Wagner F *et al* 1982 *Phys. Rev. Lett.* **49** 1408
[2] Groebner R J 1993 *Phys. Fluids* B **5** 2343
[3] Zohm H *et al* 1994 *ISPP-16, Tokamak Concept Improvement* ed S Bernabei *et al* (Bologna: SIF) p 149
[4] Ryter F *et al* 1994 *Plasma Phys. Control. Fusion* **36** A99
[5] Burrell K H *et al* 1989 *Plasma Phys. Control. Fusion* **31** 1649
[6] Doyle E J *et al* 1991 *Phys. Fluids* B **3**
[7] Gohil P *et al* 1988 *Phys. Rev. Lett.* **61**
[8] Ozeki T *et al* 1990 *Nucl. Fusion* **30** 1425
[9] Zohm H *et al* 1995 *Nucl. Fusion* **35** 543
[10] Jackson G L *et al* 1991 *Phys. Rev. Lett.* **67** 3098
[11] Osborne T H *et al* 1995 *Nucl. Fusion* **35** 23
[12] Kaufmann M *et al* 1994 *Proc. 15th Int. Conf. on Plasma Physics and Controlled Nuclear Fusion Research (Seville)* IAEA-CN-60/A4-I-1
[13] Zohm H *et al* 1992 *Nucl. Fusion* **32** 489
[14] ASDEX team 1989 *Nucl. Fusion* **29** 1959
[15] Zohm H *et al* 1995 *Proc. 22nd EPS Conf. on Plasma Physics and Controlled Fusion (Bournemouth, UK) Plasma Phys. Control. Fusion* to appear
[16] Burrell K H *et al* 1990 *Phys Fluids* B **2** 1405
[17] Zohm H 1994 *Phys. Rev. Lett.* **72** 222
[18] Gruber O *et al Phys. Rev. Lett.* **74** 4217
[19] Hutchinson I *et al* 1994 *Plasma Phys. Control. Fusion* **36** B143
[20] Snipes J 1995 *Proc. 5th H-mode Workshop (Princeton, USA) Plasma Phys. Control. Fusion* to appear
[21] Valovic M *et al* 1994 *Proc. 21st Euro. Conf. Controlled Fusion and Plasma Physics (Montpellier)* vol I p 318
[22] Buttery R *et al* 1995 *Proc. 22nd Euro. Conf. Controlled Fusion and Plasma Physics (Bournemouth, UK)*
[23] Miura Y *et al* 1991 *Proc. 13th Int. Conf. on Plasma Physics and Controlled Nuclear Fusion Research (Washington DC)*
[24] Leonard A W *et al* 1991 *Nucl. Fusion* **31** 1511
[25] Todd T N *et al* 1993 *Plasma Phys. Control. Fusion* **35** B231
[26] Colton A *et al* 1993 *Proc. 20th Euro. Conf. Controlled Fusion and Plasma Physics (Lisbon)* vol I p 11
[27] Ali-Arshad S *et al* 1992 *Proc. 19th Euro. Conf. Controlled Fusion and Plasma Physics (Innsbruck)* vol I p 227
[28] de Blank H J, Nave M F F, Kerner W and Huysmans G T A 1991 *JET-R(91)08*
[29] Campbell D *et al* 1994 *Plasma Phys. Control. Fusion* **36** A255
[30] Stork D *et al* 1994 *Plasma Phys. Control. Fusion* **36** A23
[31] Jones T *et al* 1995 *Proc. 22nd Euro. Conf. Controlled Fusion and Plasma Physics (Bournemouth, UK) Plasma Phys. Control. Fusion* to appear
[32] Parail V *et al* 1994 *Proc. 15th Int. Conf. on Plasma Physics and Controlled Nuclear Fusion Research (Seville)* IAEA-CN-60 /A-2-II-3
[33] Cordey J G *et al* 1994 *Plasma Phys. Control. Fusion* **36** A267
[34] Kaye S M *et al* 1994 *Plasma Phys. Control. Fusion* **36** A135

[35] Kaye S M *et al* 1990 *Proc. XVII Conf. Controlled Fusion and Plasma Physics (Amsterdam)* vol I p 375
[36] Weisen H *et al* 1995 *Proc. 22nd Euro. Conf. Controlled Fusion and Plasma Physics (Bournemouth, UK)*
[37] Dutch M *et al* 1995 *Nucl. Fusion* **35** 650
[38] Wagner F *et al* 1994 *Plasma Phys. Control. Fusion* **36** (1994) A61
[39] Zohm H *Proc. 5th H-mode Workshop (Princeton, USA) Plasma Phys. Control. Fusion* to appear
[40] Itoh S, Itoh K, Fukuyama A and Miura Y 1991 *Phys. Rev. Lett.* **67** 2485
[41] Itoh K 1994 *Plasma Phys. Control. Fusion* **36** A307
[42] Diamond P H *et al* 1994 *Proc. 15th Int. Conf. on Plasma Physics and Controlled Nuclear Fusion Research (Seville)* IAEA-CN-60/D-2-II-6
[43] Diamond P H, Liang Y M, Carreras B A and Terry P W 1994 *Phys. Rev. Lett.* **72** 2565
[44] Sugama H and Horton W 1995 *Plasma Phys. Control. Fusion* **37** 345
[45] Itoh K *et al* 1995 *Plasma Phys. Control. Fusion* **37** 707
[46] De Blank H J 1995 private communication
[47] Huysmans G T A, de Blank H J, Kerner W, Goedbloed J P and Nave M F F 1992 *Proc. 19th Euro. Conf. Controlled Fusion and Plasma Physics (Innsbruck)* vol I p 247
[48] Manickam J 1992 *Phys. Fluids* B **4**